JACS
JOURNAL OF THE AMERICAN CHEMICAL SOCIETY

Article

pubs.acs.org/JACS

# Increasing Stability and Activity of Core–Shell Catalysts by Preferential Segregation of Oxide on Edges and Vertexes: Oxygen Reduction on Ti–Au@Pt/C

Jue Hu,[†,§] Lijun Wu,[‡] Kurian A. Kuttiyiel,[†] Kenneth R. Goodman,[∥] Chengxu Zhang,[*,§] Yimei Zhu,[‡] Miomir B. Vukmirovic,[†] Michael G. White,[†,∥] Kotaro Sasaki,[†] and Radoslav R. Adzic[*,†]

[†]Chemistry Department and [‡]Department of Condensed Matter Physics and Materials Science, Brookhaven National Laboratory, Upton, New York 11973, United States

[§]Institute of Plasma Physics, Chinese Academy of Sciences, P.O. Box 1126, Hefei, Anhui 230031, China

[∥]Department of Chemistry, Stony Brook University, Stony Brook, New York 11794, United States

Supporting Information

**ABSTRACT:** We describe a new class of core–shell nanoparticle catalysts having edges and vertexes covered by refractory metal oxide that preferentially segregates onto these catalyst sites. The monolayer shell is deposited on the oxide-free core atoms. The oxide on edges and vertexes induces high catalyst stability and activity. The catalyst and synthesis are exemplified by fabrication of Au nanoparticles doped by Ti atoms that segregate as oxide onto low-coordination sites of edges and vertexes. Pt monolayer shell deposited on Au sites has the mass and specific activities for the oxygen reduction reaction about 13 and 5 times higher than those of commercial Pt/C catalysts. The durability tests show no activity loss after 10 000 potential cycles from 0.6 to 1.0 V. The superior activity and durability of the Ti–Au@Pt catalyst originate from protective titanium oxide located at the most dissolution-prone edge and vertex sites and Au-supported active and stable Pt shell.

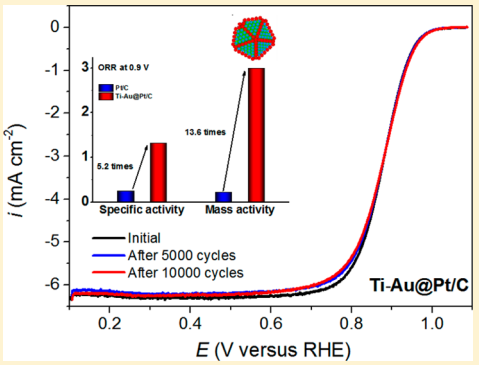


## INTRODUCTION

The slow kinetics of the oxygen reduction reaction (ORR) is one of the key obstacles for the widespread commercialization of polymer electrolyte membrane fuel cells (PEMFCs), which has been established as one of the zero-emission power sources for the future.[1−4] Platinum (Pt) is the most efficient and preferred choice electrocatalyst for the cathodic oxygen reduction.[5−7] However, the high cost and low utilization efficiency of the state-of-the-art Pt catalyst are the main obstacles for its broad application in PEMFCs. This can be resolved by the ORR catalysts having low Pt loading, high utilization efficiency, as well as high activity and durability. Intense research efforts have been focused on developing core–shell structure catalysts with Pt shell on transition metal cores.[8−10] Great efforts have been devoted to synthesize the nanosegregated crystalline multimetallic nanoframes[5] and facet-controlled Pd nanocrystals.[11] Another noteworthy core–shell catalyst system is derived from dealloying nonprecious metal to obtain a Pt-rich shell.[9,12,13] Our group has been focusing on the design and synthesis of core–shell structure catalysts and have developed a class of catalysts consisting of a Pt monolayer on different substrate metals and alloy, for example, Pd, Ru, Ir, Rh, PdAu, IrNi, IrRe, and AuNiFe.[14−20] It appears that the degradation of transition metal cores in the core–shell catalysts is the major problem under harsh fuel-cell operation conditions.[21] Our previous work also demonstrated that even Pd which is a relatively stable transition metal undergoes certain dissolution from the cores in Pd@Pt core–shell catalysts.[22]

As a non-Pt group metal (non-PGM), Au is of considerable importance in electrochemical technology, given its possibility to improve stability of various catalysts and its several times larger natural abundance than that of Pt metals.[23−25] The large-scale application of Au will be unlikely to produce unpredictable fluctuation in supply and price due to its comparatively large holding and wide distribution in the world. According to the experimental study reported in our previous work, it has been proved that depositing Au cluster on Pt surface could suppress the degradations of Pt nanoparticles.[24] Recently, Kodama and co-workers also demonstrated that Au as a vulnerable sites protector could improve the durability and activity of stepped Pt single-crystal.[26] Thus, these observations suggest a promising Au@Pt core–shell ORR catalyst with highly stable Au core and vulnerable sites protector that is generated by the spontaneous segregation of Au atoms onto the surface during electrochemical activation due to the lower surface energy of Au than Pt.[27] However, the lack of interest in the Au@Pt core–shell catalysts can be attributed to two impeding effects on ORR activity: the strong bonding of OH and O to Pt due to the up-shifts of *d*-band

**Received:** May 20, 2016
**Published:** June 30, 2016





DOI: 10.1021/jacs.6b04999
J. Am. Chem. Soc. 2016, 138, 9294−9300

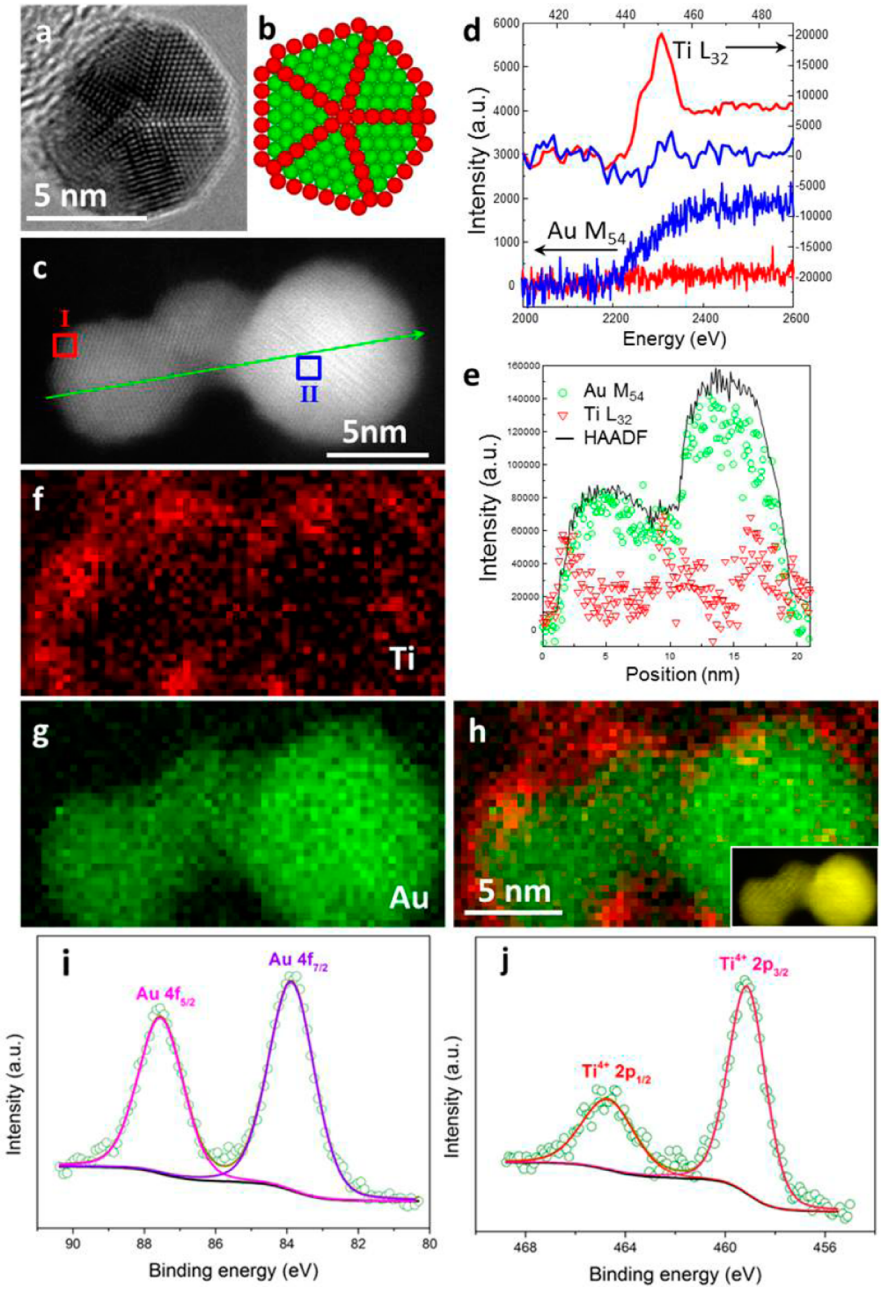


**Figure 1.** Microstructure of Ti-doped Au nanoparticles. (a) High-resolution TEM (HRTEM) image of a Ti−Au nanoparticle viewed along 5-fold axis ([110] direction in *fcc* lattice), showing five twins and truncated decahedral shape (see Supporting Information for details). (b) Schematic of a partially truncated decahedral Ti−Au multiply twined nanoparticle with Au (green spheres) at core and Ti (red spheres) at the <110> edge of the facets. (c) HAADF-STEM image, showing three nanoparticles. (d) EELS of Ti $L_{32}$ (top two lines) and Au $M_{54}$ edges (bottom two lines) from areas I (red) and II (blue) marked by corresponding red and blue squares in c, indicating that there is Ti but little Au in area I, whereas there is Au but little Ti in area II. (e) EELS signal intensity of Ti $L_{32}$ (red triangles) and Au $M_{54}$ (green circles) edges from the EELS spectrum image from the line scan indicated by the arrow in (a). Simultaneously acquired STEM-HAADF image intensity is drawn as a solid black line. (f and g) Signal intensity maps of (f) Ti $L_{32}$ and (g) Au $M_{54}$ edges from the 2D EELS spectrum image of the same particles, showing that Au is at core, whereas Ti distributes at the surface of the particles, mainly at the sharp corners. (h) Color mixture from f and g. The simultaneously acquired STEM-HAADF image is shown in the inset. (i) Au 4f and (j) Ti 2p XPS spectra of Ti−Au/C sample.

center for Pt on Au core, induced mainly by the strain effects, and the blocking of active sites of Pt due to too much Au segregation onto the Pt surface.[20,27,28] Here, we describe a novel Au@Pt core−shell catalyst with the low-coordinated surface sites doped by titanium oxide, e.g., vertex and edges, and Pt occupying the surface facets. The as-prepared Ti−Au@Pt/C has a more effective hydrogenation of $OH_{ad}$ on its Pt surface than commercial Pt/C catalyst and exhibits a 5-fold enhancement of specific activity (1.32 mA $cm^{-2}$) and 13-fold enhancement of mass activity (3.0 A $mg^{-1}$) relative to those of the commercial Pt/C catalyst. Furthermore, in the Ti−Au@Pt/C catalysts, the highly active/distorted joint edges and corners are sealed by titanium oxide that effectively prevent Au atoms from segregating onto the Pt surface and thus largely retain the electrochemical surface area (ECSA) and the ORR activity after potential cycling tests.



DOI: 10.1021/jacs.6b04999
J. Am. Chem. Soc. 2016, 138, 9294−9300

## RESULTS

In a typical synthesis of Ti-doped Au (Ti−Au) nanoparticles, Ti was first synthesized as the seeds by super-hydride reduction, followed by adding Au salt into the remaining mixture to reduce the Au salt to Au metal (see Supporting Information). The transmission electron microscopy (TEM) and high-angle annular dark-field scanning TEM (HAADF-STEM) images reveal that the Ti−Au nanoparticles on the carbon substrate are highly dispersed and have uniform size (the average size is about 6.8 nm). Most nanoparticles have polygonal shape with multiple facets (Figure S1). When the nanoparticles are viewed along <110> direction, five {111} twins are commonly observed and likely have decahedral or icosahedral shape (Figures 1a and S2).

Figure 1a shows the high-resolution TEM (HRTEM) image of a typical Ti−Au particle with truncated decahedral shape viewed along its 5-fold axis ([110] direction in the *fcc* lattice). The 5-fold {111} twins are also present in Figure S2 along with facets and edges. To obtain the distribution of Ti and Au, we performed electron energy-loss spectroscopy (EELS) analysis. Figure 1d shows the EELS spectra from the edge and interior of the particles after background subtraction, indicating uneven distribution of Ti and Au at the edge and interior of the particle. The line scan profile of the EELS signal intensity using Au $M_{54}$ and Ti $L_{32}$ edges (Figure 1e) reveals the nanostructure of the Ti−Au nanoparticles with the Au in the core, while Ti decorated on the surface. 2D EELS signal intensity maps (Figures 1f−h and S2) further reveal that Ti is mainly concentrated on the corners of the particles, indicating Ti is likely gathered at the joint edges and vertexes of the facets. DFT studies have demonstrated that molybdenum oxides prefer to segregate onto the low-coordinated sites of the Pt catalyst surface, especially at edge and vertex sites, which is reasonable because metal oxide normally has lower surface energy than the pure metal.[7] In this study, the surface energy of Au (~1130 erg/cm$^2$) is about 4 times larger than that of $TiO_2$ (280−380 erg/cm$^2$), suggesting a similar behavior of $TiO_2$-like molybdenum oxide, which prefers to segregate onto the low-coordinated sites of Au surface.[29] To further understand the nanostructure of Ti−Au nanoparticles, X-ray photoelectron spectroscopy (XPS) study was performed. The Au 4f X-ray XPS spectra (Figure 1i, Al K$\alpha$, 1486.6 eV) showed that the Au was in the metallic state ($Au^0$) by a $4f_{7/2}$ binding energy of 83.9 eV for Ti−Au/C nanoparticles.[30] Ti was present in the oxidized state ($Ti^{4+}$) by the $2p_{3/2}$ binding energy of 459.7 eV (Figure 1j). As shown in Figure S3, the O 1s spectrum for Ti−Au/C catalyst has a large portion of metal−oxygen bonds (Ti−O) with binding energy of 530.7 eV, confirming the existence of surface $TiO_2$ species, which is consistent with the EELS measurements.[31,32] Moreover, in a decahedral Au particle shown in Figure 1a, there are 10 {111} facets and 15 <110> joint edges, leaving a 1.47° gap for each edge.[33] Inhomogeneous strain or distortion of the bond length is required to produce a space-filling structure,[34] resulting in these edges becoming the preferable sites for titanium oxide. Therefore, this special elemental distribution in the Ti−Au nanoparticles could be caused by preferential segregation of titanium oxides into the low-coordinated sites, especially edges and vertexes, due to the presence of oxygen in the solution during the initial nanoparticles synthesis. The schematic in Figure 1b illustrates the atomic structure of a decahedral Ti−Au nanoparticle with Au in the core and Ti at the joint <110> edges and vertexes of the {111} facets corresponding the particle shown in Figure 1a.

To obtain a Pt shell on the as-prepared Ti−Au nanoparticle surface (Ti−Au@Pt), Cu monolayer was first formed by Cu underpotential deposition (UPD) process, followed by galvanic displacement of Cu by Pt. Figure S4 shows the TEM image and the particles size distributions of the Ti−Au@Pt/C nanoparticles. The particle size distribution shows that the mean particle size is 7.6 nm in diameter, which is slightly larger than that of Ti−Au/C nanoparticles (6.8 nm). The Au core and Pt shell structure of the Ti−Au@Pt/C catalysts is verified by the simultaneously acquired EELS and energy dispersive X-ray spectroscopy (EDS) spectrum images (Figure 2). As shown in Figure 2a,b, Au is in the core, Pt exhibits a relatively homogeneous distribution outside the particles, and Ti is concentrated at the edge and corner. The EDS spectrum image (Figure 2e) from the vertical line scan marked in Figure 2d shows that the Pt $L_\alpha$ signal extends beyond the Au $L_\alpha$ signal confirming a core−shell structure of Pt shell on the Au core.

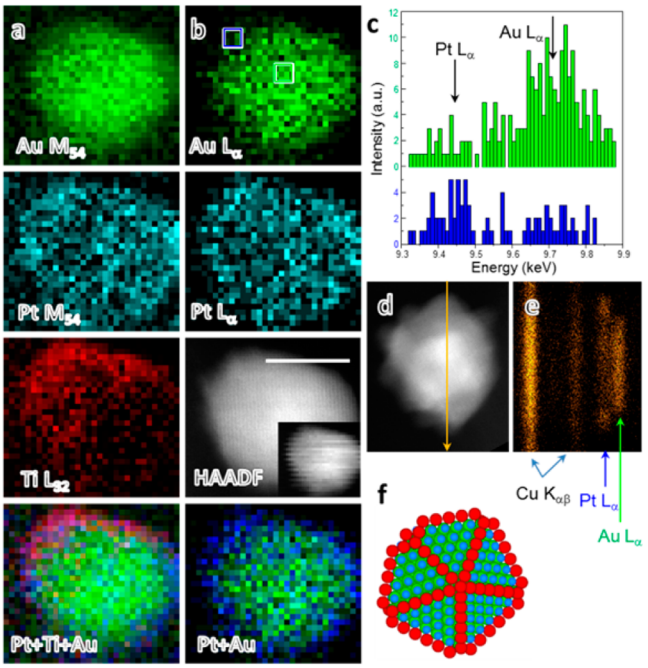


**Figure 2.** Microstructure of Ti−Au@Pt core−shell nanoparticles. (a) EELS and (b) EDS signal intensity of Au (first row, green), Pt (second row, light blue), and Ti (third row in b, red) from simultaneously acquired EELS and EDS spectrum image from a Ti−Au@Pt nanoparticle (b, third row). The simultaneously acquired STEM-HAADF image is shown in the inset in the third row in b. The scale bar in third row of b is 5 nm. The fourth row in a is the combined color image using EELS Au signal as green component, Pt signal as blue component, and Ti signal as red component, whereas that in b is combined using EDS Au (green) and Pt (blue) signals. (c) EDS spectra from the core (green bars) and edge (blue) of the particle. The area is marked in the first row in b with the same colored squares. (d) STEM-HAADF image of a Ti−Au@Pt nanoparticle. (e) EDS spectrum image from the line scan (arrow) in d. The length of the line scan is 15 nm. The Cu $K_{ab}$ signals come from the Cu grid background. The EDS spectrum image in e and Au, Pt, and Ti signal mapping in a and b clearly show that Pt and Ti are on the surface, whereas Au is in the core. Pt is basically uniformly distributed on the surface, whereas Ti is mainly at sharp corner. (f) Schematic of Ti−Au@Pt nanoparticle with Au (green spheres) in core, Ti (red spheres) at joint of the facets, and Pt on the surface facets.


DOI: 10.1021/jacs.6b04999
J. Am. Chem. Soc. 2016, 138, 9294−9300

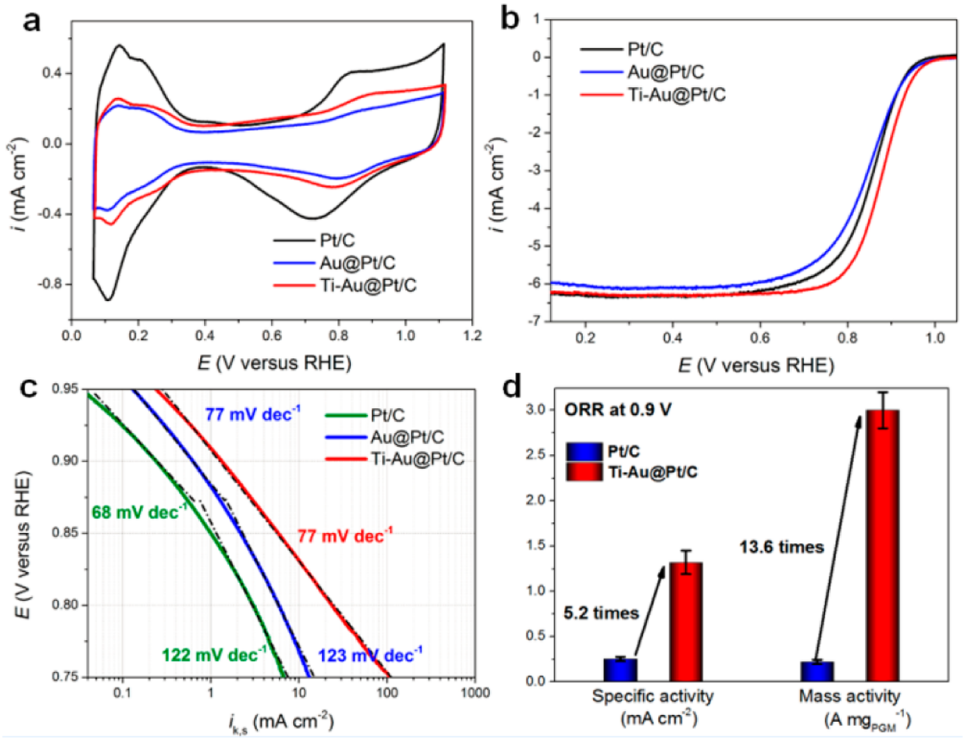


**Figure 3.** Electrocatalytic properties of Ti−Au@Pt/C catalysts. (a) Cyclic voltammograms of Ti−Au@Pt/C, Au@Pt/C, and commercial Pt/C recorded in Ar-saturated 0.1 M $HClO_4$ solution with a scan rate of 50 mV $s^{-1}$ at room temperature. (b) Corresponding ORR polarization curves recorded in $O_2$-saturated with a rotation rate of 1600 rpm and a scan rate of 10 mV $s^{-1}$. Pt loadings for Ti−Au@Pt/C, Au@Pt/C, and commercial Pt/C catalysts were 1.1, 1.3, and 9.7 $\mu$g $cm^{-2}$ respectively. (c) Mass transport corrected Tafel plots based on specific current density for Au@Pt/C, Ti−Au@Pt/C, and commercial Pt/C catalysts obtained from ORR polarization curves. (d) Comparison of specific activities and mass activities at 0.9 V for Ti−Au@Pt/C and commercial Pt/C. Error bars show the variation of three sets of experimental repeats.

Because Pt atoms cannot be deposited on the titanium oxide surface by the Cu UPD method, it is reasonable that Pt shell only covers the facets of the Au atoms and the titanium oxides remain at the joint edges of the particle surface as evidenced in the third and fourth rows of Figure 2a,b where Ti is mainly distributed at the sharp edges and corners. The schematic of a decahedral Ti−Au@Pt nanoparticle with Au (green sphere) in the core, Pt (blue) on the surface facets, and Ti (red) at the joint edges of the facets is depicted in Figure 2f.

Cyclic voltammograms (CVs) recorded in Ar-saturated 0.1 M $HClO_4$ solution (Figure 3a) reveal that the hydrogen adsorption/desorption ($H_{upd}$) and oxide species adsorption/desorption regions resembles those of Pt/C surface. A slight positive shift of the potential of the oxide reduction peak was observed for Ti−Au@Pt/C catalyst compared with commercial Pt/C, indicating a decrease of desorption free energy of oxide species from Pt surface and a stabilization of Pt on the Ti−Au/C substrate.[35−37] The ORR polarization curves for Ti−Au@Pt/C, Au@Pt/C, and the commercial Pt/C catalysts as thin films on a rotating disk electrode (RDE) in $O_2$-saturated 0.1 M $HClO_4$ solution at 1600 rpm are shown in Figure 3b. The value of diffusion current density indicates a complete reduction of $O_2$ to $H_2O$ (a four-electron process) on the surface of the Ti−Au@Pt/C catalyst.[38,39] The half wave potential ($E_{1/2}$) in the ORR polarization curve for Ti−Au@Pt/C core−shell catalyst, which processes only one-ninth of the Pt loading of commercial Pt/C, is 25 mV higher than that of commercial Pt/C, indicating a much higher activity for Ti−Au@Pt/C core−shell catalyst.[40] The half-wave potential is only an indicator of ORR activity but not a true measure of it, so Pt specific and mass activities at 0.9 V were calculated using the Koutecky−Levich equation and then normalized with respect to both the ECSA ($i_{k,s}$) and the amount of Pt loading ($i_{k,m}$). ECSA calculated by measuring the charge associated with the $H_{upd}$ region between 0.05 and 0.35 V after double-layer charging correction and assuming a value of 210 $\mu$C $cm^{-2}$ for adsorption of a hydrogen monolayer.[7] As shown in Figure S6, both the specific activity and mass activity of the Ti−Au@Pt/C catalyst were clearly enhanced relative to the commercial Pt/C, verifying the accelerated ORR kinetics on the Ti−Au@Pt/C surface.[41] Figure 3d compares the specific activity and mass activity for Ti−Au@Pt/C (1.32 mA $cm^{-2}$ and 3.0 A $mg^{-1}$) and commercial Pt/C (0.254 mA $cm^{-2}$ and 0.22 A $mg^{-1}$) catalysts at 0.9 V. The mass activity of the Ti−Au@Pt/C catalyst exhibits 13-fold enhancement over that of commercial Pt/C catalyst, whereas the specific activity achieves a 5-fold improvement. Considering that Au is a nonplatinum group metal, the PGM-based mass activities for the Ti−Au@Pt/C and Au@Pt/C catalysts are equal to the Pt-based mass activities. To get a deeper insight of this unexpected enhancement of the ORR activity on the distinct titanium oxide doped Pt surface, mass transport corrected Tafel plots based on specific current density ($i_{k,s}$) for Ti−Au@Pt/C and Au@Pt/C were analyzed. As shown in Figure 3c, a low Tafel slope of −77 mV $dec^{-1}$ was fitted for both the Ti−Au@Pt/C and Au@Pt/C catalysts at the high potential region from 0.95 to 0.85 V, which is in close agreement with that of commercial Pt/C catalyst, indicating a similar ORR pathway with pure Pt surface at the high potential region. Typically, the Tafel plot on pure Pt surface in 0.1 M $HClO_4$ solution was well-fitted with two Tafel slopes: a lower Tafel slope at the high potential region and a higher Tafel slope


DOI: 10.1021/jacs.6b04999
J. Am. Chem. Soc. 2016, 138, 9294−9300

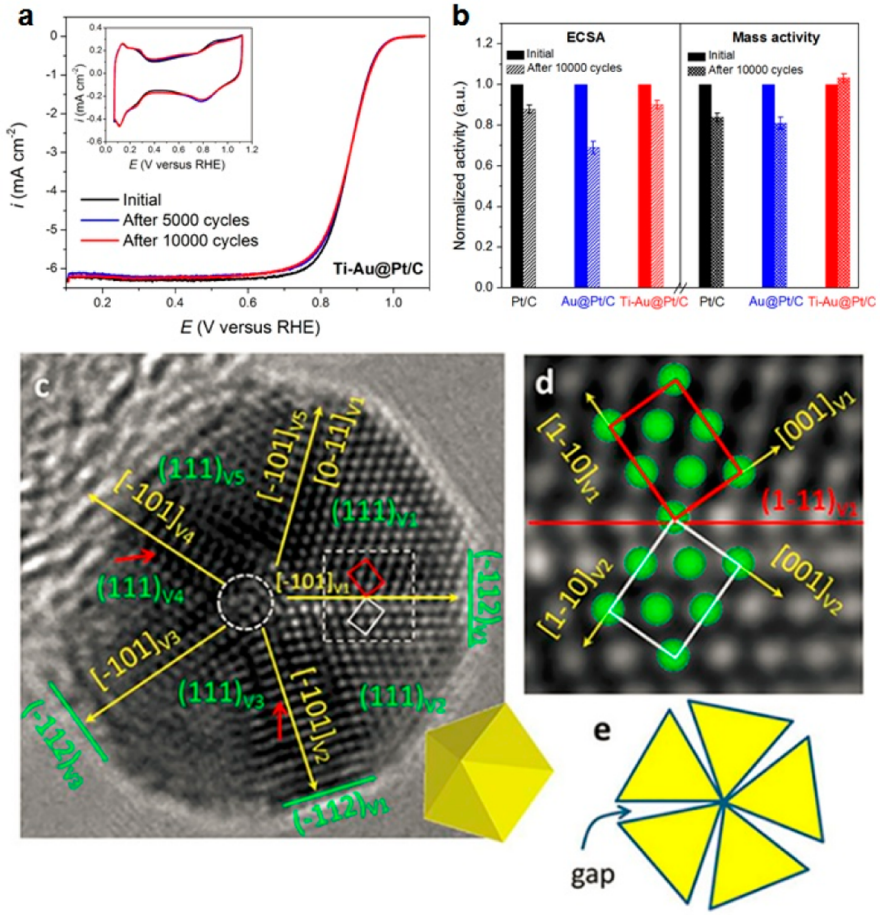


**Figure 4.** Electrochemical durability of the catalysts. (a) ORR polarization curves and (inset) corresponding cyclic voltammgrams of Ti−Au@Pt/C catalyst before and after 10 000 potential cycles between 0.6 and 1.0 V. (b) Losses of ECSAs (left) and mass activities (right) at 0.9 V of the Au@Pt/C, Ti−Au@Pt/C, and the commercial Pt/C catalysts after 10 000 potential cycles between 0.6 and 1.0 V. (c) High-resolution TEM (HRTEM) image of a Ti−Au nanoparticle viewed along [110] direction, showing five twins and truncated decahedral shape. A decahedron is shown in the inset. The yellow arrows (the joint edges of the facets) are the vectors from the center apex to the bottom apexes. The scale bar is 5 nm. (d) Magnified image from the area marked by white dash square in c. (e) Schematic diagram of a perfect *fcc* tetrahedral subunit viewed along [110] direction.

**Table 1. Comparison of Electrochemical Activity and Durability of Au@Pt/C, Ti−Au@Pt/C and the Commercial Pt/C Catalysts**

| catalyst | | Pt loading ($\mu$g cm$^{-2}$) | ECSA (m$^2$ g$^{-1}_{Pt}$) | $E_{1/2}$ (mV) | specific activity (mA cm$^{-2}$) at 0.9 V | mass activity (A mg$_{PGM}^{-1}$) at 0.9 V | mass activity (A mg$_{Pt+Au}^{-1}$) at 0.9 V |
|---|---|---|---|---|---|---|---|
| Pt/C | initial | 9.7 | 86.6 | 853 | 0.254 | 0.22 | 0.22 |
| | after 10000 cycles | | 76.2 | 846 | 0.243 | 0.185 | 0.185 |
| Au@Pt/C | initial | 1.3 | 194.7 | 845 | 0.63 | 1.21 | 0.08 |
| | after 10000 cycles | | 134.4 | 834 | 0.72 | 0.98 | 0.065 |
| Ti−Au@Pt/C | initial | 1.1 | 225.4 | 878 | 1.32 | 3.00 | 0.35 |
| | after 5000 cycles | | 211.8 | 878 | 1.44 | 3.05 | 0.35 |
| | after 10000 cycles | | 203.2 | 878 | 1.53 | 3.10 | 0.36 |

at the low potential region.[42] It can be also clearly observed from Figure 3c that the Tafel slopes for both Au@Pt/C and commercial Pt/C catalysts increase at the low potential region. The increase of Tafel slope at the low potential region was attributed to the sluggish ORR kinetics by the site-blocking and electronic effects of adsorbed $OH_{ad}$ on the Pt surface.[42−44] $OH_{ad}$ removal from Pt surface, which has been shown to be the rate-determining step of ORR for Pt-based catalysts, is crucial to improve the catalysts' performance.[6,45,46] Damjanovic et al. attributed the two slopes to a change from Temkin to Langmuir adsorption conditions for reaction intermediates with decreasing coverage.[47] At high current densities for Pt/C catalyst, coverage with oxygen is negligible, and the kinetics under Langmuir conditions result in a high Tafel slope. At higher potentials, oxygen and coverage increases, and the Temkin conditions become operative: The current density decreases, which results in a low Tafel slope. Markovic et al. explained this behavior as being due to a change in the surface


DOI: 10.1021/jacs.6b04999
J. Am. Chem. Soc. 2016, 138, 9294−9300

coverage of the chemisorbed oxygen-containing species that affect the adsorption of $O_2$ on Pt.[48] On the basis of these observations, no change in the Tafel slope at high current density for the Ti-doped Au@Pt catalyst seems to indicate that it is caused by the Temkin conditions created by the repulsive interaction of the titanium oxide species. DFT calculations have also demonstrated that the destabilization of $OH_{ad}$ on Pt, which can be attributed to the repulsive interaction between the $OH_{ad}$ on Pt and the oxide species on a neighboring Ti,[46] is responsible for enhancing the ORR kinetics, and at the same time possesses increased stability of Ti−Au@Pt/C catalyst under typical fuel cell operating condition.

In addition to the high electrochemical activities, the Ti−Au@Pt/C catalyst also exhibited excellent durability (Figures 4 and S7). The durability of the Ti−Au@Pt/C catalyst was evaluated using accelerated durability test (ADT) by potential cycling between 0.6 and 1.0 V for 10 000 cycles in air-saturated 0.1 M $HClO_4$ solution at a scan rate of 50 mV $s^{-1}$. For comparison, the durability of Au@Pt/C and commercial Pt/C catalysts were also measured under the same conditions, as shown in Table 1 and Figure S8. As illustrated, after 10 000 cycles, the commercial Pt/C catalyst exhibited 8 mV shifts for its half-wave potential and 16% loss of its initial mass activity due to the dissolution of Pt atoms and agglomeration of Pt nanoparticles through surface oxidation/reduction processes.[5] In contrast, during the potential cycling, the Ti−Au@Pt/C catalyst largely retained its activity, exhibiting no loss for its half-wave potential. Furthermore, after 10 000 cycles, the mass activity of Ti−Au@Pt/C catalyst is still as high as 3.10 A $mg^{-1}$. The mass activity and specific activity of the Ti−Au@Pt/C catalyst after 10 000 cycles exhibit a 13-fold and 5-fold enhancement over the initial performance of commercial Pt/C catalyst, respectively. The changes of ECSA and mass activity for Ti−Au@Pt/C, Au@Pt/C, and commercial Pt/C catalysts were further examined by normalizing with respect to their initial ECSA and mass activity at 0.9 V, as shown in Figure 4b. It is worth noticing that Ti−Au@Pt/C catalyst retained its ECSA, whereas Au@Pt/C suffered the largest ECSA loss (31%) after 10 000 cycles among these three catalysts. Our previous study demonstrated that the movement of Au atoms from core to the defective sites gains high energy, resulting in Au atoms preferentially residing on the surface low-coordinated sites (such as edge and vertex sites) by segregation process.[28] The Au segregation process will mend the defective sites on the Pt surface inhibiting the dissolution; moreover, a little bit of Au on the Pt surface could further confer catalyst durability by raising the Pt oxidation potential.[24,49] However, too many segregated Au atoms on the Pt surface will block the Pt active sites, resulting in a big loss of ECSA of the Au@Pt/C catalyst and, of course, a decrease of catalyst performance.

## DISCUSSION

Density functional theory (DFT) calculations indicate that there is a stronger driving force for metal oxide to segregate onto the catalyst surface relative to metal and form metal oxide species on the surface low-coordinated sites, especially on edge and vertex sites which are considered to be the most stable surface sites for metal oxide.[7] The decahedral and icosahedral Au nanoparticles with {111} twins are commonly obtained by different synthesis methods.[34,50,51] For a decahedral Au particle, there are 10 {111} facets and 15 <110> joint edges. If the vertexes are truncated, then an additional five $(\bar{1}12)$ and two (110) facets form, as shown in Figure 4c. The unit cell of the Au twin variants V1 and V2 are outlined by red and white rectangles, respectively. The [110] projection of the Au atoms of the twin variants V1 and V2 is embedded in Figure 4d. Clearly, V2 is related with V1 by $(1\bar{1}1)$ reflection twin. On the basis of *fcc* $(1\bar{1}1)$ reflection twin relation, the angle between the twin variants is 70.53°, so five of them would take a total of 352.65°, leaving a 7.35°/5 = 1.47° gap for each edge, as shown in Figure 4e.[33] Inhomogeneous strain or distortions of the bond length is required to produce a space-filling structure, as indicated by the red arrows.[34,52] The distortion required for a decahedral particle with 5-fold twins corresponds to a simple angular gap or wedge disclination, as shown in the area circled in a dashed line in Figure 4c. We think that these edges are the preferable sites for titanium oxide, as confirmed by EELS composition map. Pt then covers Au surface facets, e.g., {111} facets. This core−shell structure would be more stable than that without titanium oxide coating because the highly active/distorted joint edges with gap are sealed by titanium oxide for preventing Au from coming to the surface, thus improvings the ORR durability. The much smaller ECSA loss for Ti−Au@Pt/C catalyst than that for Au@Pt/C catalyst after 10 000 cycles demonstrated the contribution of titanium oxide to improved durability by preventing Au atoms from segregating onto the Pt surface. Moreover, as a result of the propensity for metal oxide segregation on its thermodynamically favored low-coordinated sites, titanium oxide in the Ti−Au@Pt/C catalyst was located at low-coordinated vertex and edge sites on the catalyst surface, inhibiting the dissolution of the catalyst.

## CONCLUSIONS

We described a promising new class of Pt-based catalysts having high activity and high durability for the ORR obtained by depositing Pt shell on titanium oxide doped Au core. EELS and XPS analyses proved the distinct microstructure of Ti−Au@Pt nanoparticles with Au as the core, Pt as the shell, and protective titanium oxide located in the highly active/distorted edge and vertex sites of the nanoparticles. The as-prepared Ti−Au@Pt/C catalyst possessed a more effective hydrogenation of $OH_{ad}$ on its Pt surface than that of commercial Pt/C catalyst and exhibits high ORR performance with a mass activity of 3.0 A $mg^{-1}_{Pt}$ and a specific activity of 1.32 mA $cm^{-2}_{Pt}$, which are 13- and 5-fold enhancements compared with those of commercial Pt/C catalyst. Furthermore, in the Ti−Au@Pt/C catalysts, titanium oxide doped on the Au@Pt surface effectively prevents Au atoms from segregating onto the Pt surface and thus can largely retain the ECSA and ORR activity of Ti−Au@Pt/C catalyst after 10 000 potential cycles.

## ASSOCIATED CONTENT

### Supporting Information

The Supporting Information is available free of charge on the ACS Publications website at DOI: 10.1021/jacs.6b04999.

Experimental details and characterization data (TEM, size distribution, HAADF-STEM, XPS , mass activities, cyclic voltammetry, and ORR polarization curves) (PDF)

## AUTHOR INFORMATION

### Corresponding Authors

*chxzhang@ipp.ac.cn

*adzic@bnl.gov

### Notes

The authors declare no competing financial interest.



DOI: 10.1021/jacs.6b04999
J. Am. Chem. Soc. 2016, 138, 9294−9300

## ■ ACKNOWLEDGMENTS

This manuscript has been authored by employees of Brookhaven Science Associates, LLC, under Contract No. DE-SC0012704 with the U.S. Department of Energy. J.H. acknowledges the support by the National Nature Science Foundation of Anhui Province (No. 1508085QA10) and the Youth Innovation Promotion Association of Chinese Academy of Sciences (No. 2015265).

## ■ REFERENCES

(1) Gasteiger, H. A.; Markovi, N. M. *Science* **2009**, *324*, 48.
(2) Debe, M. K. *Nature* **2012**, *486*, 43.
(3) Stamenkovic, V. R.; Fowler, B.; Mun, B. S.; Wang, G.; Ross, P. N.; Lucas, C. A.; Marković, N. M. *Science* **2007**, *315*, 493.
(4) Hernandez-Fernandez, P.; Masini, F.; McCarthy, D. N.; Strebel, C. E.; Friebel, D.; Deiana, D.; Malacrida, P.; Nierhoff, A.; Bodin, A.; Wise, A. M.; Nielsen, J. H.; Hansen, T. W.; Nilsson, A.; Stephens, I. E. L.; Chorkendorff, Ib. *Nat. Chem.* **2014**, *6*, 732.
(5) Chen, C.; Kang, Y.; Huo, Z.; Zhu, Z.; Huang, W.; Xin, H. L.; Snyder, J. D.; Li, D.; Herron, J. A.; Mavrikakis, M.; Chi, M.; More, K. L.; Li, Y.; Markovic, N. M.; Somorjai, G. A.; Yang, P.; Stamenkovic, V. R. *Science* **2014**, *343*, 1339.
(6) Zhang, L.; Roling, L. T.; Wang, X.; Vara, M.; Chi, M.; Liu, J.; Choi, S.-I.; Park, J.; Herron, J. A.; Xie, Z.; Mavrikakis, M.; Xia, Y. *Science* **2015**, *349*, 412.
(7) Huang, X.; Zhao, Z.; Cao, L.; Chen, Y.; Zhu, E.; Lin, Z.; Li, M.; Yan, A.; Zettl, A.; Wang, Y. M.; Duan, X.; Mueller, T.; Huang, Y. *Science* **2015**, *348*, 1230.
(8) Wang, D. L.; Xin, H. L. L.; Hovden, R.; Wang, H. S.; Yu, Y. C.; Muller, D. A.; DiSalvo, F. J.; Abruna, H. D. *Nat. Mater.* **2012**, *12*, 81.
(9) Strasser, P.; Koh, S.; Anniyev, T.; Greeley, J.; More, K.; Yu, C. F.; Liu, Z. C.; Kaya, S.; Nordlund, D.; Ogasawara, H.; Toney, M. F.; Nilsson, A. *Nat. Chem.* **2010**, *2*, 454.
(10) Wang, D.; Xin, H. L.; Yu, Y.; Wang, H.; Rus, E.; Muller, D. A.; Abruña, H. D. *J. Am. Chem. Soc.* **2010**, *132*, 17664.
(11) Xie, S.; Choi, S.-I.; Lu, N.; Roling, L. T.; Herron, J. A.; Zhang, L.; Park, J.; Wang, J.; Kim, M. J.; Xie, Z.; Mavrikakis, M.; Xia, Y. *Nano Lett.* **2014**, *14*, 3570.
(12) Oezaslan, M.; Heggen, M.; Strasser, P. *J. Am. Chem. Soc.* **2012**, *134*, 514.
(13) Wu, Y.; Wang, D.; Niu, Z.; Chen, P.; Zhou, G.; Li, Y. *Angew. Chem., Int. Ed.* **2012**, *51*, 12524.
(14) Wang, J. X.; Inada, H.; Wu, L. J.; Zhu, Y. M.; Choi, Y. M.; Liu, P.; Zhou, W. P.; Adzic, R. R. *J. Am. Chem. Soc.* **2009**, *131*, 17298.
(15) Karan, H. I.; Sasaki, K.; Kuttiyiel, K.; Farberow, C. A.; Mavrikakis, M.; Adzic, R. R. *ACS Catal.* **2012**, *2*, 817.
(16) Zhang, Y.; Hsieh, Y. C.; Volkov, V.; Su, D.; An, W.; Si, R.; Zhu, Y. M.; Liu, P.; Wang, J. X.; Adzic, R. R. *ACS Catal.* **2014**, *4*, 738.
(17) Zhang, Y.; Ma, C.; Zhu, Y. M.; Si, R.; Cai, Y.; Wang, J. X.; Adzic, R. R. *Catal. Today* **2013**, *202*, 50.
(18) Kuttiyiel, K. A.; Sasaki, K.; Choi, Y.; Su, D.; Liu, P.; Adzic, R. R. *Energy Environ. Sci.* **2012**, *5*, 5297.
(19) Hsieh, Y.-C.; Zhang, Y.; Su, D.; Volkov, V.; Si, R.; Wu, L.; Zhu, Y.; An, W.; Liu, P.; He, P.; Ye, S.; Adzic, R. R.; Wang, J. X. *Nat. Commun.* **2013**, *4*, 2466.
(20) Zhang, J.; Vukmirovic, M. B.; Xu, Y.; Mavrikakis, M.; Adzic, R. R. *Angew. Chem., Int. Ed.* **2005**, *44*, 2132.
(21) Yang, H. *Angew. Chem., Int. Ed.* **2011**, *50*, 2674.
(22) Sasaki, K.; Naohara, H.; Cai, Y.; Choi, Y. M.; Liu, P.; Vukmirovic, M. B.; Wang, J. X.; Adzic, R. R. *Angew. Chem., Int. Ed.* **2010**, *49*, 8602.
(23) Corti, C.; Holliday, R.; Thompson, D. *Gold Bull.* **2002**, *35*, 111.
(24) Zhang, J.; Sasaki, K.; Sutter, E.; Adzic, R. R. *Science* **2007**, *315*, 220.
(25) Maroun, F.; Ozanam, F.; Magnussen, O. M.; Behm, R. J. *Science* **2001**, *293*, 1811.
(26) Kodama, K.; Jinnouchi, R.; Takahashi, N.; Murata, H.; Morimoto, Y. *J. Am. Chem. Soc.* **2016**, *138*, 4194.
(27) Ruban, A. V.; Skriver, H. L.; Nørskov, J. K. *Phys. Rev. B: Condens. Matter Mater. Phys.* **1999**, *59*, 15990.
(28) Sasaki, K.; Naohara, H.; Choi, Y. M.; Cai, Y.; Chen, W. F.; Liu, P.; Adzic, R. R. *Nat. Commun.* **2012**, *3*, 1115.
(29) Zhang, L.; Persaud, R.; Madey, T. E. *Phys. Rev. B: Condens. Matter Mater. Phys.* **1997**, *56*, 10549.
(30) Zhang, P.; Sham, T. K. *Phys. Rev. Lett.* **2003**, *90*, 245502.
(31) Hu, J.; Jiang, L.; Zhang, C.; Zhang, X.; Meng, Y.; Wang, X. *Appl. Phys. Lett.* **2014**, *104*, 151602.
(32) Duan, J.; Hu, J.; Xu, L.; Wen, Y.; Zhang, C.; Meng, Y.; Zhang, C. *Plasma Sci. Technol.* **2015**, *17*, 303.
(33) Johnson, C. L.; Snoeck, E.; Ezcurdia, M.; Rodriguez-Gonzalez, B.; Pastoriza-Santos, I.; Liz-Marzan, L. M.; Hytch, M. J. *Nat. Mater.* **2008**, *7*, 120.
(34) Wang, Z. L. *J. Phys. Chem. B* **2000**, *104*, 1153.
(35) Zhao, X.; Chen, S.; Fang, Z.; Ding, J.; Sang, W.; Wang, Y.; Zhao, J.; Peng, Z.; Zeng, J. *J. Am. Chem. Soc.* **2015**, *137*, 2804.
(36) Hu, J.; Kuttiyiel, K.; Sasaki, K.; Su, D.; Yang, T.-H.; Park, G.-G.; Zhang, C.; Chen, G.; Adzic, R. *Catalysts* **2015**, *5*, 1321.
(37) Van der Vliet, D. F.; Wang, C.; Li, D.; Paulikas, A. P.; Greeley, J.; Rankin, R. B.; Strmcnik, D.; Tripkovic, D.; Markovic, N. M.; Stamenkovic, V. R. *Angew. Chem.* **2012**, *124*, 3193.
(38) Wang, C.; Daimon, H.; Onodera, T.; Koda, T.; Sun, S. *Angew. Chem., Int. Ed.* **2008**, *47*, 3588.
(39) Niu, W.; Li, L.; Liu, X.; Wang, N.; Liu, J.; Zhou, W.; Tang, Z.; Chen, S. *J. Am. Chem. Soc.* **2015**, *137*, 5555.
(40) Kuttiyiel, K. A.; Sasaki, K.; Choi, Y. M.; Su, D.; Liu, P.; Adzic, R. R. *Nano Lett.* **2012**, *12*, 6266.
(41) Escudero-Escribano, M.; Verdaguer-Casadevall, A.; Malacrida, P.; Grønbjerg, U.; Knudsen, B. P.; Jepsen, A. K.; Rossmeisl, J.; Stephens, I. E. L.; Chorkendorff, I. *J. Am. Chem. Soc.* **2012**, *134*, 16476.
(42) Wang, J. X.; Markovic, N. M.; Adzic, R. R. *J. Phys. Chem. B* **2004**, *108*, 4127.
(43) Marković, N. M.; Gasteiger, H. A.; Grgur, B. N.; Ross, P. N. *J. Electroanal. Chem.* **1999**, *467*, 157.
(44) Wang, J. X.; Zhang, J.; Adzic, R. R. *J. Phys. Chem. A* **2007**, *111*, 12702.
(45) Greeley, J.; Stephens, I. E. L.; Bondarenko, A. S.; Johansson, T. P.; Hansen, H. A.; Jaramillo, T. F.; Rossmeisl, J.; Chorkendorff, I.; Nørskov, J. K. *Nat. Chem.* **2009**, *1*, 552.
(46) Zhang, J.; Vukmirovic, M. B.; Sasaki, K.; Nilekar, A. U.; Mavrikakis, M.; Adzic, R. R. *J. Am. Chem. Soc.* **2005**, *127*, 12480.
(47) Damjanovic, A.; Genshaw, M. A. *Electrochim. Acta* **1970**, *15*, 1281.
(48) Markovic, N. M.; Adzic, R. R.; Cahan, B. D.; Yeager, E. B. *J. Electroanal. Chem.* **1994**, *377*, 249.
(49) Kuttiyiel, K. A.; Sasaki, K.; Su, D.; Vukmirovic, M. B.; Marinkovic, N. S.; Adzic, R. R. *Electrochim. Acta* **2013**, *110*, 267.
(50) Zheng, Y.; Tao, J.; Liu, H.; Zeng, J.; Yu, T.; Ma, Y.; Moran, C.; Wu, L.; Zhu, Y.; Liu, J.; Xia, Y. *Small* **2011**, *7*, 2307.
(51) Johnson, C. J.; Dujardin, E.; Davis, S. A.; Murphy, C. J.; Mann, S. *J. Mater. Chem.* **2002**, *12*, 1765.
(52) Marks, L. D. *Rep. Prog. Phys.* **1994**, *57*, 603.



DOI: 10.1021/jacs.6b04999
*J. Am. Chem. Soc.* 2016, 138, 9294−9300